The Effects of Reynolds Number on Flow Separation of Naca Aerofoil

Open Access

Muhammad Syahmi Abdul Hakim[1], Mastura Ab Wahid[1,*], Norazila Othman[1], Shabudin Mat[1,♣], Shuhaimi Mansor[1], Md. Nizam Dahalan[1], Wan Khairuddin Wan Ali[1]

[1] Department of Aeronautical, Automotive and Offshore Engineering, Fakulti Kejuruteraan Mekanikal, Universiti Teknologi Malaysia, 81310 Skudai, Johor, Malaysia

ARTICLE INFO	ABSTRACT
	The purpose of this study is to investigate the flow separation above UTM 2D Airfoil at three different Reynolds numbers which are 1×10^6, 1.5×10^6 and 2×10^6 using pressure distribution method and flow visualization. The experiment was conducted in UTM-LST (Low Speed Tunnel). The pressure distribution is done on three different wing span, which are 40%, 50% and 70%m of span and was measured and plotted to observe the flow characteristic at angle of attack from 0° to 35° for all three different Reynolds numbers. The flow visualization method was done at 10m/s, 20m/s and 30m/s airspeed from 0° to 18°. It is concluded that the Reynolds number of 1×10^6 separates at 16°; Reynolds number of 1.5×10^6 separates at 18° and Reynolds number of 2×10^6 separates at 20°.

1. Introduction

1.1 Flow Separation

Many researchers [1, 11, 12, 20] stated that for normal case of airfoil, there will be a pressure acting on the forward (leading-edge) surface. For attached flow case, the pressure on the aft surface (trailing edge) produces a net force to counter back the leading-edge force, so that there will be no pressure drag. But it is different for separated flow case, where the pressure acting on the aft surface will be insufficient to counter back the pressure acting on the forward surface. In this case, a net pressure drag will be produced in the direction towards the aft surface therefore reducing the speed.

---

* *Corresponding authors*
E-mail address: mastura@mail.fkm.utm.my (Mastura Ab Wahid)
♣ *Corresponding authors*
E-mail address: shabudin@fkm.utm.my (Shabudin bin Mat)

1.2 Adverse Pressure Gradient

According to Basu [2], adverse pressure gradient is one of the important terms that should be noted in order to investigate flow separation. Adverse pressure gradient is a region where the pressure increases in the flow direction, where the region dP/dx (pressure gradient) is positive. Adverse pressure gradient occurs when the static pressure increases in the direction of the flow. In boundary layer condition, adverse pressure gradient causes the velocity of boundary layer to reduce; therefore, the kinetic energy of the fluid particles is no longer adequate to move the particles against the pressure gradient. This situation causes flow reversal for the layers nearer to the wall or object surface. However, the layers further from the wall are uninterrupted, which produces more energy. Flow reversal at the lower parts and further energetic flow at the upper parts causes the fluid streams to roll and separate from the wall, as explained by Munson [14].

1.3 Types of Stalls

According to few researchers [2, 10, 13 and 18], it has been observed leading-edge stall occurs in airfoil characteristics, such as thin airfoil with the thickness ratio between 10% and 16% of the chord length. For all stall cases, the stagnation point is moved downward at the leading-edge as the angle of attack (AOA) increases. However, for leading-edge stall, the flow separation originates at leading-edge causing the flow to separate all over the top surface of the airfoil. As contrast to leading-edge stall, trailing-edge stall is due to thicker types of airfoil. For this type of stall, flow separate originates from the trailing-edge. The separation point moves towards the leading-edge as the AOA is increased. It was noted that the trailing-edge stall is softer than leading-edge stall but having lower maximum coefficient of lift value. Thin airfoil stall is for very thin airfoil, which is defined as flat plate with thickness at 2% of airfoil chord length. This case is unique because it visualizes both types of stall which are leading-edge and trailing-edge stalls. At first, flow begins to separate at leading-edge even at low AOA, but due to extreme thickness of airfoil, the flow reattaches back further downstream which forms a separation bubble. This separation bubble phenomenon becomes larger with the increase of AOA due to the reattachment point moving further downstream. These three kinds of stalls are based on statement from Anderson et al. [1] in his book of aerodynamics. In this research, an experimental investigation on aerodynamics characteristic about the flow separation above a 2-dimensional (2D) airfoil has been performed, which investigates the flow separation above UTM 2D Wing at three different Reynolds Number - 1×10^6, 1.5×10^6 and 2×10^6.

1.4 Experimental Methods

Experimental method is used in order to identify how the flow separates and effect of different Reynolds Number to the flow separation. There are many flow visualization methods that have been perform such as oil method, smoke-wire method, particle image velocimetry and tuft thread method as in refs. [6,7,11,19 and 22], however according to John [4], tuft method is the best method for photographic evidence as it provides clear view, easy to apply and to analyze. As mentioned Tajuddin *et al.*, [21], the flow separation and air flow formation around the blunt-edged delta wing can be easily observed. Shen *et al.*, [19] stated that this technique can be used on both steady state flows as well as time varying flow fields, and complements a host of flow visualization techniques. In a steady flow field, each tuft is subjected to a constant wind force. As a result, the tuft can be observed to swing periodically. The direction of motion is the same as the flow field. The resulting tuft shows the changing orientation of the tuft as the vector field. In other words, the tufting method allows the

invisible wind forces to be observed since its reactions are exerted onto the set of yarn, thread or even in the digital analysis virtual tuft.

The method records the movement on the top surface of airfoil, and will be recorded by camera. Pressure distribution taps are used to monitor and the result will be used to support the data from flow visualization. Shahrul Sham Dol [5] stated that flow visualization is an important method in order to study the flow behaviour around objects including airfoil. In contrast of other methods, flow visualization is capable in delivering a qualitative macroscopic picture of the overall flow field instead of limitations from measuring flow conditions at discrete point within the flow field. Flow visualization is important to identify the flow pattern above the airfoil in various conditions which help to identify airfoil characteristic during the test. Basically, airfoil is tested in different angle of attack (AOA) until stalling effect occurs which is the critical value for the airfoil to obtain maximum coefficient of lift. The airfoil behaviour can be represented in coefficient of lift, C_L vs. Angle of attack, α graph consists of the linear part and stalling part. But since the project is about flow separation, the flow visualization is more focused on the stalling part. There is also another parameter that is controlled in order to visualize the flow over an airfoil using the Reynolds number. Reynolds number is integrated with the free stream speed that will affect the type of flow acting to the airfoil where this parameter need to be controlled in order to visualize the result that is being predicted.

2. Methodology

The model used is UTM 2D wing with symmetrical airfoil to the specification of NACA 0012. Since the main focus of this project is to investigate the flow separation, the project was carried out by using the methods of pressure distribution and flow visualization. The infinite wing model is mounted inside the test section of UTM-LST, Low Speed Tunnel. Take note that the wing is tilted at a set of angles of attack from 0° to 35° which covers the stall angle of attack. This is because the stall angle of attack provides better flow separation visualization. Other parameters are added such as the wind speed and Reynolds Number. The model is tested with three different set of Reynolds Number which are 1.0×10^6, 1.5×10^6 and 2.0×10^6 respectively. These parameters help in order to understand better about the effect of Reynolds Number to the flow separation.

The pressure distribution method was carried out through the pressure taps on the airfoil model surface. Pressure distribution method provides local pressure data for each point around the airfoil in order to identify the presence of adverse pressure gradient. Adverse pressure occurrence indicates how much flow separation occurs and in locating the separation points on the top surface of the airfoil. Pressure gradient or dP/dx equal to zero shows that there is constant pressure on the region where flow is separated resulting to no pressure difference and can be observed by this method focusing on the flat pressure plateau region. On top of that, point of separation could be observed either occurring upstream or downstream the transition point, indicating laminar or turbulent separation. The data is recorded by the Lab View application on the wind tunnel facility with the help of portable electronic pressure scanner.

Using the tuft method as the flow visualization method is created using the tuft method as this method is most suitable with the current facilities available, where sets of threads are mounted on the top surface of the model. These sets of threads are mounted span wise of the airfoil at each of the model chord so that the flow could be analyzed accordingly. Thread tuft technique is used in order to study the flow direction since the tuft react on the forces produced by the flow strength itself. Therefore, in the case of flow separation, there is no force acting on the tuft and reversed flow will cause the tuft to point to the reverse direction of the upstream test section of the air flow. This method is advantageous since it provides visual data in which the flow behaviour could be observed.

The data is recorded by camera and observed manually to compare results as gained by the pressure distribution method. The experimental flow chart is shown in Figure 1.
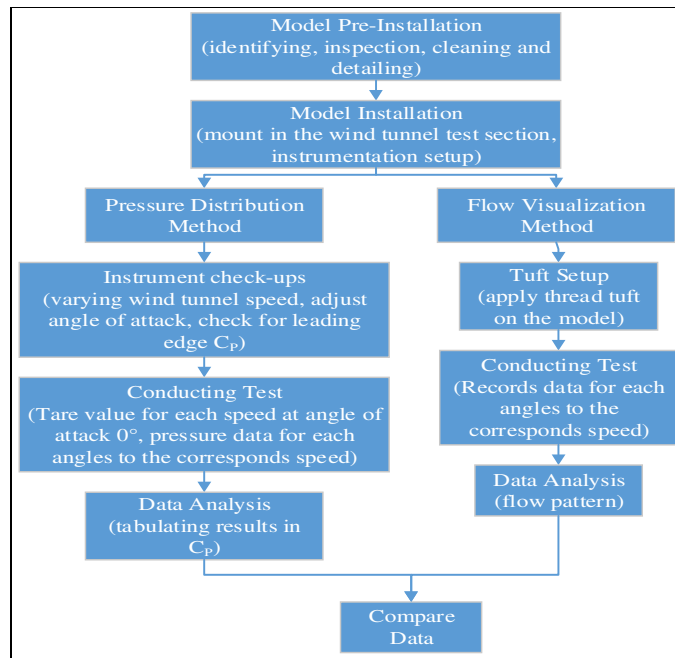
Fig. 1. Experimental Process Flow Chart

The test configurations for Pressure distribution method and Flow Visualization via Tuft method are shown in Table 1 and Table 2.

Table 1
Flow visualization Test Configuration

Span 1 (40% of model span)		Span 2 (50% of model span)		Span 3 (70% of model span)	
Airspeed	Angle	Airspeed	Angle	Airspeed	Angle
30.60 m/s,	0° to 35°	30.60 m/s,	0° to 35°	30.60 m/s,	0° to 35°
30.90 m/s	0° to 30°	30.90 m/s	0° to 30°	30.90 m/s	0° to 30°
60.20 m/s	0° to 24°	60.20 m/s	0° to 24°	60.20 m/s	0° to 24°

Table 2
Tuft Method: Wind-On Tuft testing configuration

Airspeed	Angle of attack
10 m/s	0° to 18°
20 m/s	0° to 18°
30 m/s	0° to 18°

2.1 UTM Half Model Specification

The model used in this project is the UTM 2D Wing Model which consists of symmetrical aero foil to the specification of NACA 0012. The span of the model is 1,476 mm, comfortably set in the wind tunnel test section with the height of 1.5 m as shown in Figure 2 and Figure 3. The model will be

mounted and balanced in the middle of the test section that can be turned into different angles of attack by the turntable. The chord length of the wing is 500 m and consists of 96 pressure taps. Since this wing is a symmetrical wing, both upper and lower section will have the same amount of 16 pressure taps at the exact same location. The top and bottom surface for each span consist of 40%, 50% and 70% of wing span as shown in Table 4. Note that all the pressure taps are aligned at the same distance for each span as the wing model is mounted vertically across the flow field (Figure 2).

Fig. 2. UTM half model
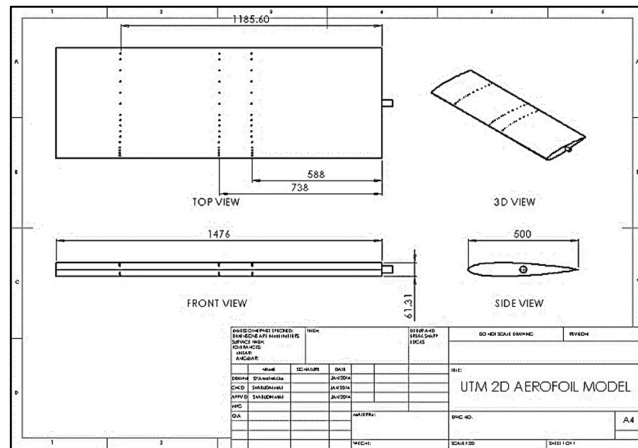
Fig. 3. The dimension of the UTM half model

Table 3
Specifications of the UTM 2D Wing Model

UTM 2D WING MODEL SPECIFICATION	
Aerofoil	NACA 0012
Wing Span	1476 mm
Chord Length	500 m
Max Thickness	12% at 30% chord (60 mm)
Number of Pressure Taps	96 (32 for each span and 16 on each span)
Location of Pressure Taps	40% span (588 mm), 50% span (738 mm)and 70% span (1,038 mm) from the tunnel floor

3. Results and Analysis

3.1 Pressure Distribution Method

The desired Reynolds Number can be controlled by manipulating the airspeed inside the wind tunnel section. Recall that the required set of Reynolds Number in this test is 1 million, 1.5 million and 2 million. Take 1 million Re for example and using Reynolds Number formula

$$Re = \frac{\rho V l}{\mu} \tag{1}$$

where V is velocity, l is mean aerodynamic chord of the model, ρ is air density and V is dynamics viscosity. The known value of the air density, mean aerodynamic chord and kinematic viscosity is constant and by adjusting the formula, certain value of the wind speed can be calculated for certain value of Reynolds number. Table 5 gives the Airspeed corresponding to each Reynolds number

Table 4
UTM 2D Wing Model Pressure Tap Locations

Tap	X direction (chord wise)	Z direction (thickness)	Tap	X direction (chord wise)	Z direction (thickness)
1	12.5	13.1	16	475.0	-4.0
2	25.0	17.8	17	12.5	-13.1
3	37.5	21.0	18	25.0	-17.8
4	50.0	23.4	19	37.5	-21.0
5	75.0	26.7	20	50.0	-23.4
6	100.0	28.7	21	75.0	-26.7
7	125.0	29.7	22	100.0	-28.7
8	150.0	30.0	23	125.0	-29.7
9	175.0	29.7	24	150.0	-30.0
10	200.0	29.0	25	175.0	-29.7
11	250.0	26.5	26	200.0	-29.0
12	300.0	22.8	27	250.0	-26.5
13	350.0	18.3	28	300.0	-22.8
14	400.0	13.1	29	350.0	-18.3
15	450.0	7.2	30	400.0	-13.1

In the pressure distribution method, data obtained from this method is the local pressure at each point. Pressure coefficient is an important parameter since it shows relative pressure throughout the whole flow field and the way to analyze incompressible flow. Through this parameter it provides the general overview on the local static pressure difference to the ratio of dynamic pressure, which is calculated by using equation (2)

$$C_P = \frac{P - P_\infty}{\frac{1}{2}\rho_\infty V_\infty^2}$$ (2)

where P is the local static pressure for each of pressure taps data while P_∞ is the wind tunnel test section static pressure. ρ_∞ is the wind tunnel air density, and V_∞ is the current wind tunnel airspeed for each of Reynolds number.

Table 5
Wind tunnel airspeed calculated from the required
Reynolds number

Reynolds Number	Airspeed Velocity (m/s)
1 000 000	30.60
1 500 000	45.90
2 000 000	61.20

The first data for Span 1, sited 40% of the wing span at 30.60m/s, resulting to pressure distribution of the upper surface and offered observable changes that are distinct. Starting with angle of attack 0°, we can observe that pressure starts to decrease from pressure coefficient (C_p) of -1 (point 15 with C_P = -1.0888) at the stagnation point at the location of 15% of the wing chord. Then the static pressure continues to increase gradually to the value of pressure coefficient slightly above free-stream pressure at the trailing-edge of point 30% with C_P = -0.9478. This result corresponds with Anderson [1], where this kind of pressure distribution offers no flow separation conditions, where the adverse pressure gradient is moderate as the flow remains attached to the airfoil surface. Note that this kind of situation applies to all of the Reynolds Number of 1×10^6, 1.5×10^6 and 2×10^6, since its symmetrical airfoil shape does not contribute to any changes to the lift produced by this kind of

airfoil. As the angle of attack increases, which is to 14°, the pressure continues to decrease to their negative peaks at the location towards the airfoil leading-edge. The surface pressure gradually and smoothly recovered over the upper surface of the airfoil up to the airfoil trailing edge, as in [20] which describe how flow remains attached for all speeds.

At the angle of attack 16° as shown is the Figure 4-6, it is observed that there is the sudden drop of C_P value indicating to leading-edge stall. According to Anderson [1], thin airfoil with 10% to 16% of thickness ratio will have flow separation over the entire top surface where the origin of this separation occurs at leading-edge, and the lift curve is sharp-peaked shape due to rapid decrease in lift coefficient. The airfoil itself has 12% of thickness ratio so that leading-edge stall is predicted to occur. In the pressure distribution data, we can observe that there is existence of a region with constant pressure with no pressure differences (pressure plateau region). This starts to happen and it indicates that the flow begins to separate. In this situation, the pressure becomes constant due to the effect of adverse pressure gradient, in which the pressure increases rapidly and at this pressure plateau region shows that the increase of drag overrule the slight increase portion of lift in the leading-edge.

At this region constant pressure also causes the pressure gradient of dP/dx to be 0, therefore there is no pressure difference. Pressure difference plays a major role to ensure the flow attached to the surface. According to Munson [14], dP/dx = 0 marks the point where the flow starts to separate from the surface. This situation of no pressure difference occurs where there is no net force produced to hold or stick the flow down onto the surface, which causes the flow to be separated.
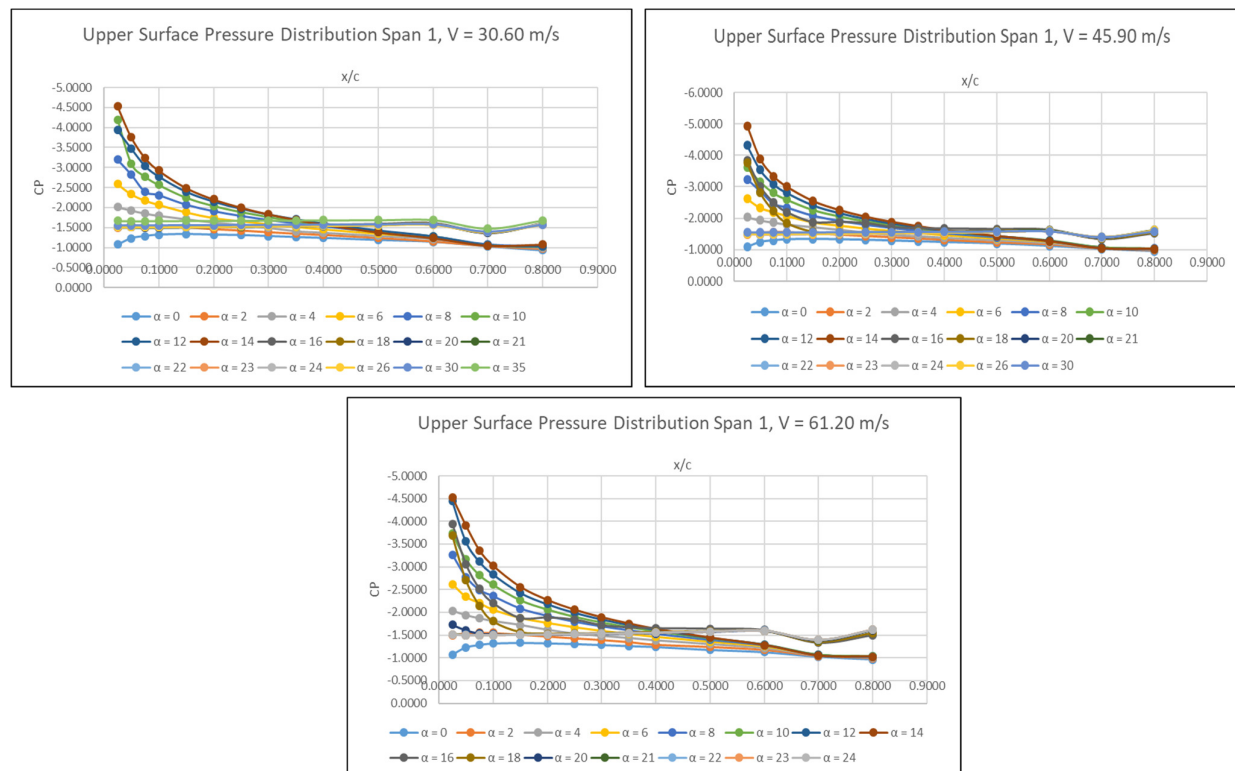
Fig. 4. Upper surface coefficient of lift distribution for 40% span at v = 30.60m/s, 45.90 m/s, 61.20m/s
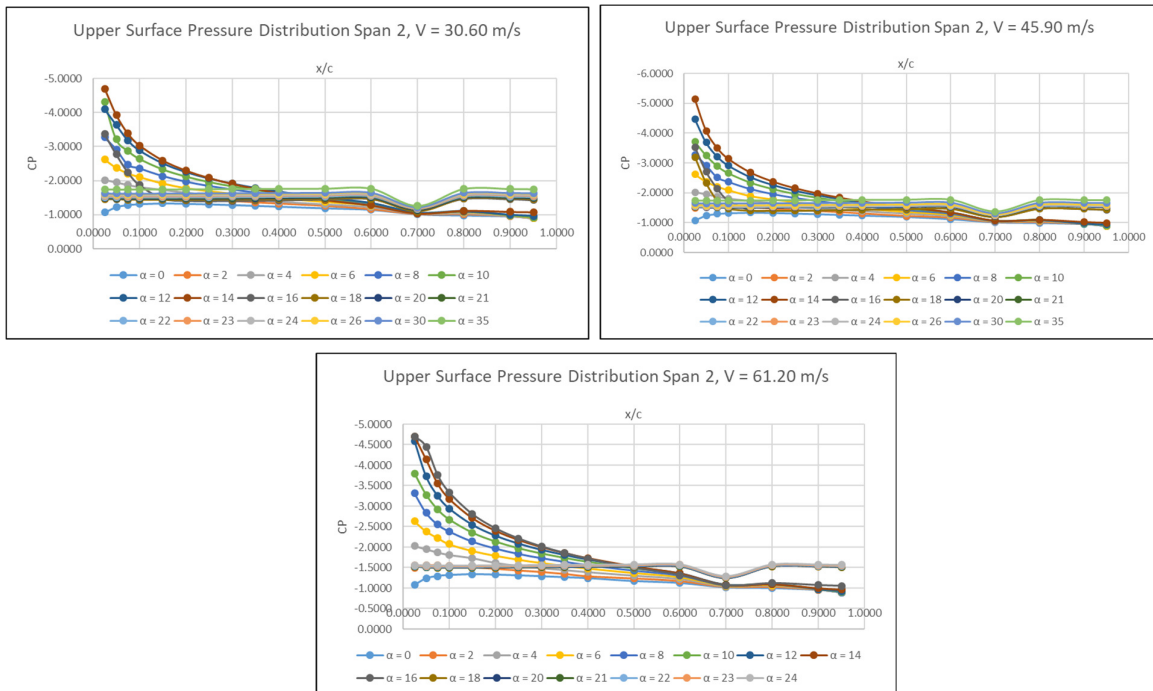
Fig. 5. Upper surface coefficient of lift distribution for 50% span at v = 30.60m/s, 45.90 m/s, 61.20m/s
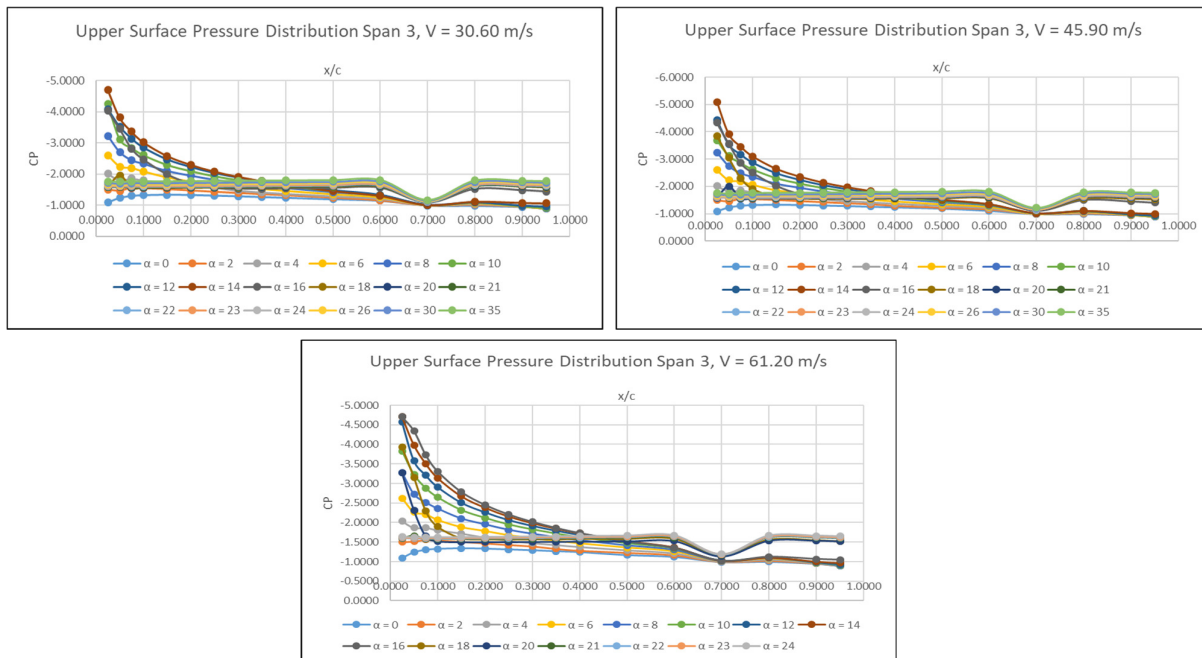
Fig. 6. Upper surface coefficient of lift distribution for 70% span at v = 30.60m/s, 45.90 m/s, 61.20m/s

Instead, for leading-edge stall such as the result predicted, we observed that small portion of the leading-edge (15% of airfoil chord) still have their flow intact and remains attached. Although it is predicted that the flow is separated from the leading-edge, it was found that high flow of energy which is above 1 million Reynolds number causes the flow to remain attached at leading-edge up to 15% of chord. Note that this situation is applied up to high angle of attack (20°), where Reynolds number of 1×10^6 is fully separated at 16° followed by Reynolds number of 1.5×10^6 fully

separating at 20°. This situation occurs when there is constant pressure distribution at the upper surface which resulted to no pressure differences, and thus no lift is generated.

However, from Figure 7, at the angle of attack 20° shows us that the coefficient of lift, C_L, rose after stall at 16° which is due to forces at the lower surface. This kind of force is due to the rising pressure at the lower surface of the airfoil (Figure 8) during high speed in which it creates pressure differences sufficient enough to increase the coefficient of lift. Note that during this angle of attack, although lift could be generated there is total separation of upper surface flow causing the drag value to exceed the lift value.

According to Anderson [1], there will be two consequences of flow separation either stall or major increase in drag which is caused by pressure drag. Thus, flow starts to separate where pressure plateau region starts to develop as seen in Figure 9. This indicates stalling conditions of the airfoil with total flow separation on the upper surface where there is constant pressure chord wise, which also indicates major increase of drag.

The three figures shown in Figure 9, provide better illustration on how the Reynolds Number tend to delay the flow separation. Based on the Figure 9 for V= 30.60m/s it can be seen that the pressure coefficient peaked at 16° angle of attack during Reynolds number of 1×10^6 and then rapidly falls due to flow separation to α = 20°.

Referring to the same figure of V = 45.90, the pressure coefficient peaked at α = 18° and starts to fall down. However, at the angle of attack between 18° to 20°, the flow separation was slightly delayed until it reaches α = 21°, where the pressure coefficient becomes fully flat. With the increase of airspeed velocity up to 61.20 m/s, the flow separation delayed further to α = 20° until reaching α = 21° where the sudden drop of pressure coefficients to a constant value, which can be observed in Figure 8 accordingly. This data also tallies with lift coefficient, where the flow separation starts, indicating the airfoil is undergoing stall conditions.
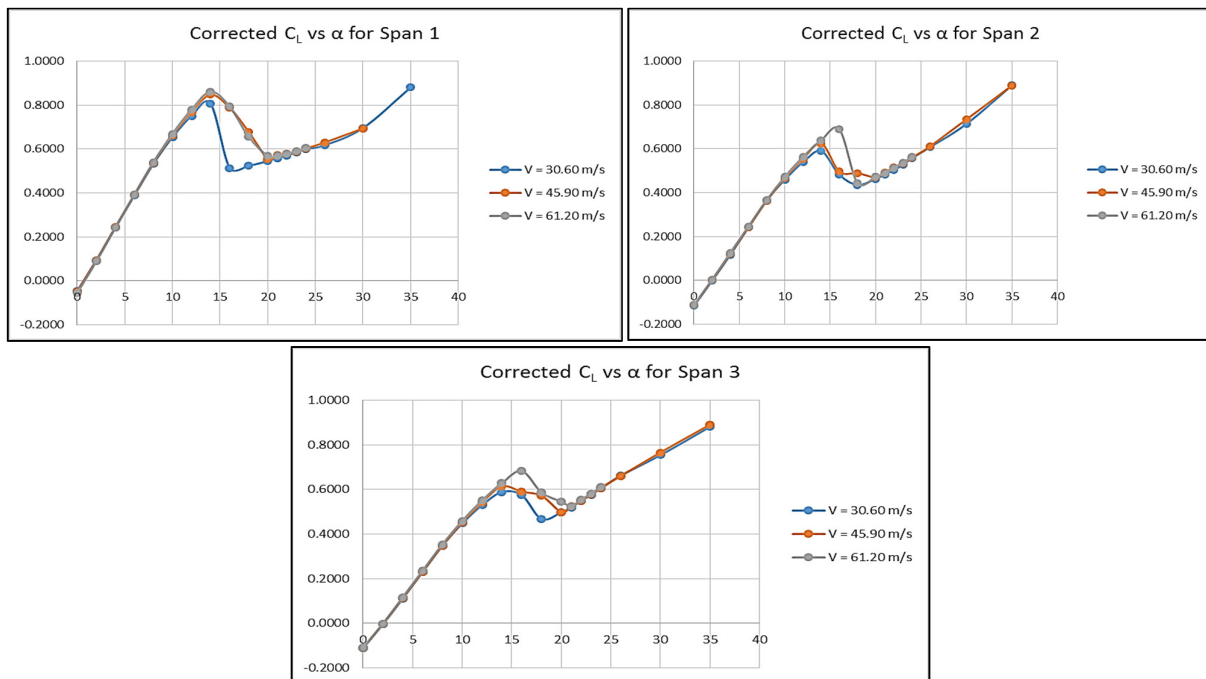
Fig. 7. Coefficient of lift for all span
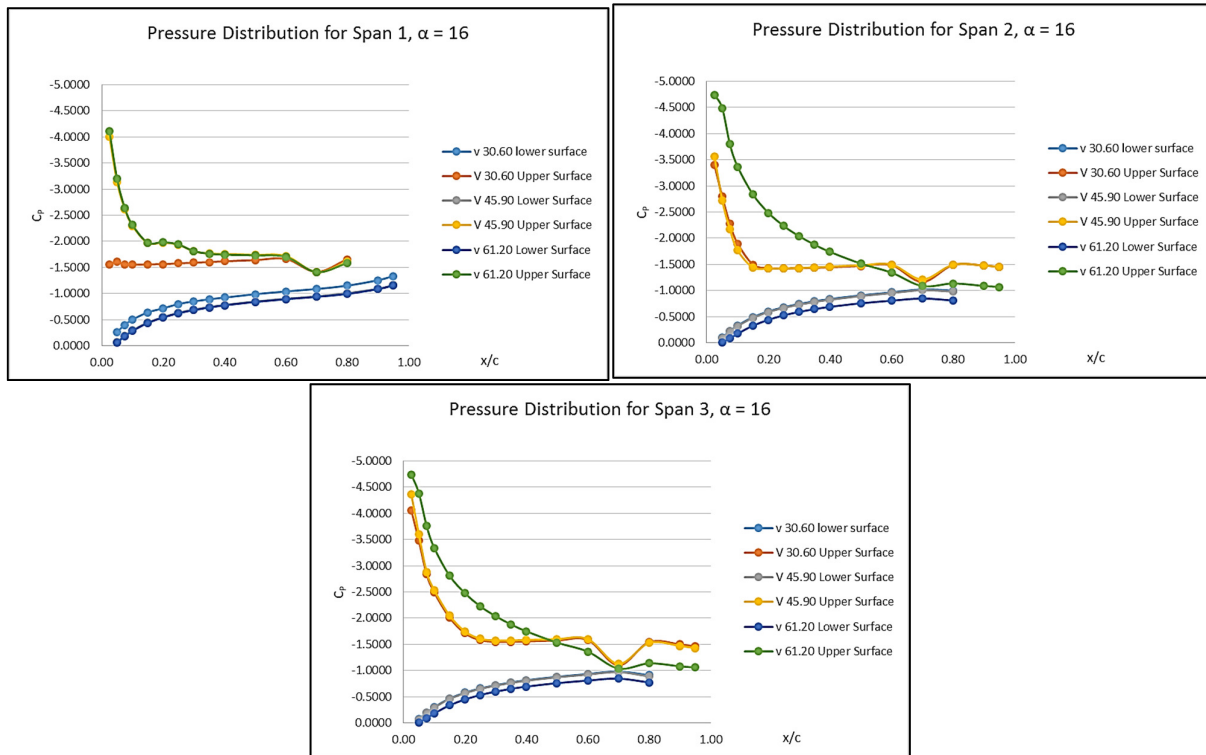
Fig. 8. V = 30.60 m/s starts flow separations for all span
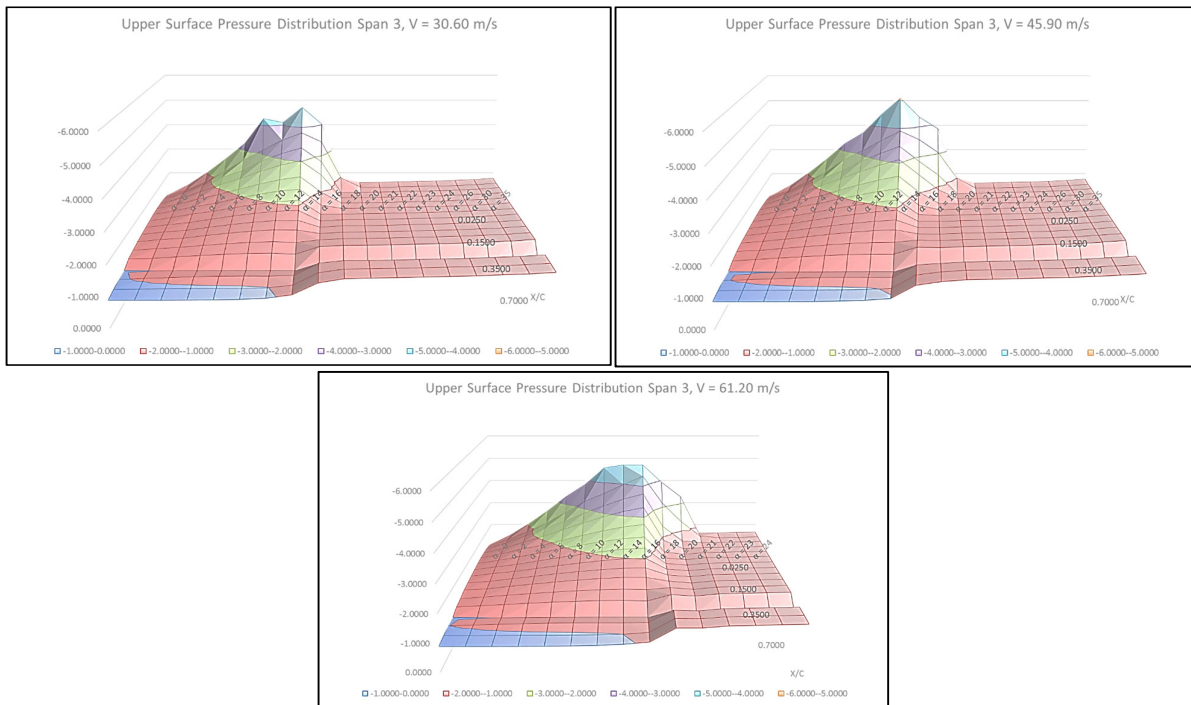
Fig. 9. Peak area shows the Reynolds number delaying flow separation

3.2 Flow Visualization Method: Tuft Method

Figure 10 shows the photographic results obtained from tuft testing for the flow visualization. In Figure 10a, it can be observed that the flow condition is fully attached as indicated by the straight orientation of the thread tuft following the free stream air flow direction. In this case, forces from the free stream of air are sufficient to act upon the tuft so as to keep the thread from falling down. In both chord positions, the thread tuft remains in a straight formation due to the flow being fully attached to the airfoil surface.

a) Tuft Test at V = 10 m/s Angle of Attack 0°

b) Tuft Test at V = 10 m/s Angle of Attack 9°

c) Tuft Test at V = 10 m/s Angle of Attack 14°

d) Tuft Test at V = 20 m/s Angle of Attack 15°

e) Tuft Test at V = 30 m/s Angle of Attack 16°

f) Reversed flow condition during tuft testing

Fig. 10. Tuft Test for different airspeed and different angle of attack

As the angle of attack increases to 9° for V = 10 m/s, the flow starts to separate from the leading-edge, as seen in the Figure 10b. At the trailing-edge of the airfoil model, the tuft thread starts to fall down with slightly a number of yarns tangling to each other. This situation interprets that the flow at the back of the airfoil is insufficient so that it possesses enough force to the yarn in order to keep them straight to the free stream air. The set of yarn starts to fall down due to the effect of gravitational forces exerted on them. It can be said that the flow in this regime has become constant due to adverse pressure gradient which denotes the insufficiency of fluid kinetic energy to attach them to the surface of the airfoil. It is observed that the flow is still attached at the front side of the airfoil model, even with the upstream flow of the leading-edge model still in straight formation.

Higher angle of attack up to 14° which can be seen in the Figure 10c shows that the total flow separation occurs on the top surface of the wing model during V = 10 m/s. This situation can be observed with the tuft threads pointed in the reverse direction to the free stream air vector. Reversed flow occurred fully on the top surface of the wing due to wake, vortex and reverse circulation present on this regime. On top of that, the tuft also became tangled which describes the unpredictable and violent nature of the turbulent flow which in turn contribute to stall occurrence. This phenomenon best presented in the Figure 10c, where the tuft threads pointed out at different directions to the free stream air vector.

By increasing the Reynolds number during the thread tuft method, the flow separation can be seen to be delayed. As higher energy flow is exerted, the flow was attached further when the angle of attack of flow velocity is increased. This situation can be observed in the Figure 10d and Figure 10e where the flow separation is delayed by 1° when the airspeed is increased by 10 m/s in increment accordingly. Interestingly, at V = 30 m/s, the flow separation occurs at angle of attack 16° which was the same angle of attack for the pressure distribution method during the occurrence of the constant pressure plateau at the trailing-edge of the airfoil during V = 30.60 m/s. This data comparison conforms that the flow separation phenomenon happens at approximate V = 30 m/s when the flow starts to separate at α = 16° and separates from the trailing edge. Thus, this situation adheres and validates the data for pressure distribution method which is accurate enough to be compared with the tuft flow visualization technique in order to provide better understanding of the flow separation behavior.

4. Conclusions

A low speed wind tunnel study is carried on the UTM 2D airfoil model in the range of 0° to 35° angle of attack at Reynolds number 1.0×10^6, 1.5×10^6 and 2.0×10^6. It can be concluded that the Reynolds number of 1.0×10^6 separates at 16°; and as the Reynolds number is increased; the flow separation could be delayed. Flow fully separates for Reynolds number of 1.5×10^6 at 18° and Reynolds number of 2.0×10^6 at 20° accordingly. As the formation of laminar separation bubble with the flow separation beyond transition point, it is found that the flow has laminar separation for all Reynolds numbers. Pressure coefficient distribution tends to be constant after high positive pressure gradient, contributing to unsteady flow due to adverse pressure gradient. Also, from the pressure distribution method shows stall conditions of the airfoil happen during the occurrence of flow separation. On top of that, by comparing the tuft visualization method and the pressure distribution data shows similar data especially during V = 30 m/s, where the flow separation occurs at α = 16° proving the validity of data from both methods. Additionally, the angle of attack beyond flow separation caused the flow to be fully reversed in the tuft flow visualization.

Acknowledgement

References

[1]   Anderson Jr, John David. *Fundamentals of aerodynamics*. Tata McGraw-Hill Education, 2010.
[2]   Asada, Kengo, Yoshihiko Ninomiya, Kozo Fujii, and Akira Oyama. "Airfoil flow experiment on the duty cycle of DBD plasma actuator." In *47th AIAA Aerospace Sciences Meeting including The New Horizons Forum and Aerospace Exposition*, p. 531. 2009.
[3]   Basu, P. "Boundary layer with pressure gradient." *Greenfield Research Inc., 18. Greenfield Research Inc*, 2001.
[4]   John D. Bird. "Visualization of flow fields by use of a tuft grid technique." *Journal of the Aeronautical Sciences* 19, no. 7 (1952): 481-485.
[5]   Blackwell, Tommy James. "Subsonic Wind-Tunnel Wall Corrections On A Wing With A Clark Y-14 Airfoil." *A Masters Project Presented to The Faculty of the Department of Mechanical and Aerospace Engineering San Jose State University* (2011).
[6]   Chen, Wen-King. "Visualization of the flow around a pitching airfoil using the smoke-wire technique." PhD diss., University of Texas at Arlington, 1990.
[7]   Dol, Sharul Sham, MOHD ARIEF MOHD Nor, and M. K. Kamaruzaman. "An improved smoke-wire flow visualization Technique." In *Proceedings of the 4th WSEAS International Conference on Fluid Mechanics and Aerodynamics*, pp. 21-23. 2006.
[8]   Genç, M. Serdar, İlyas Karasu, and H. Hakan Açıkel. "An experimental study on aerodynamics of NACA2415 aerofoil at low Re numbers." *Experimental Thermal and Fluid Science* 39 (2012): 252-264.
[9]   Genc, M. Serdar, and Ünver Kaynak. "Control of laminar separation bubble over a NACA2415 aerofoil at low re transitional flow using blowing/suction." In *13th International Conference on Aerospace Sciences & Aviation Technology*. 2009.
[10]   Gregory, Nigel, and C. L. O'reilly. *Low-Speed aerodynamic characteristics of NACA 0012 aerofoil section, including the effects of upper-surface roughness simulating hoar frost*. London: HM Stationery Office, 1973.
[11]   Hu, Hui, and Zifeng Yang. "An experimental study of the laminar flow separation on a low-Reynolds-number airfoil." *Journal of Fluids Engineering* 130, no. 5 (2008): 051101.
[12]   McArthur, John. *Aerodynamics of wings at low Reynolds numbers: boundary layer separation and reattachment*. University of Southern California, 2008.
[13]   Mulleners, Karen, A. Hemireg, and Markus Raffel. "Investigations of a Trailing Edge stall on 2D airfoils." In *14th International Symposium on Application of Laser Technology to Fluid Mechanics*, no. EPFL-CONF-218235. 2008.
[14]   Munson, Bruce R., Theodore H. Okiishi, Alric P. Rothmayer, and Wade W. Huebsch. "Fundamentals of fluid mechanics." *John Wiley & Sons,* 2014.
[15]   Pátek Z., Cervinka J. and Vrchota P. "WIND TUNNEL AND CFD STUDY OF AIRFOIL WITH AIRBRAKE". 28th international congress of aeronautical sciences (2012)
[16]   William, H., and P. Alan. "Low speed wind tunnel testing." *J. Wiley and Son, New York* (1984).
[17]   Sata.tamu.edu, *"UTM Low Speed Wind Tunnel Facility (UTM-LST),* (2001)". [online] Available at: http://sata.tamu.edu/members/tunnels/UTM.html [Accessed 30 Sep. 2013].
[18]   Sharma, Deepakkumar M., and Kamal Poddar. "Investigation of dynamic stall characteristics for flow past an oscillating airfoil at various reduced frequencies by simultaneous PIV and surface pressure measurements." In *PIV13; 10th International Symposium on Particle Image Velocimetry, Delft, The Netherlands, July 1-3, 2013*. Delft University of Technology, Faculty of Mechanical, Maritime and Materials Engineering, and Faculty of Aerospace Engineering, 2013.
[19]   Shen, Wei, and Alex Pang. "Tuft flow visualization." In *Proceedings of the Second IASTED International Conference on Visualization, Image, and Image Processing*, vol. 2002, pp. 705-710. 2002.
[20]   Yang, Zifeng, Fred Haan, Hui Hu, and Hongwei Ma. "An experimental investigation on the flow separation on a low-Reynolds-number airfoil." In *45th AIAA aerospace sciences meeting and exhibit*, p. 275. 2007.
[21]   Tajuddin, N., Mat, S., Said, M., & Mansor, S. "Flow characteristic of blunt- edged delta wing at high angle of attack." *Journal of Advanced Research in Fluid Mechanics and Thermal Sciences 39* (2017): 17-25.
[22]   Norazila O., Shabudin M., Mastura A.W., Shuhaimi M., M. Nizam D. "Experimental Study of UTM New Sport Complex." *Journal of Advanced Research in Fluid Mechanics and Thermal Sciences 40* (2017): 70-78.